ISSN: 2278-4632
Vol-13, Issue-03, No.02, March 2023

BACK-TO-BACK VOLTAGE-SOURCE CONVERTERS FOR GRID-CONNECTED WIND-SOLAR COGENERATION

Dr. J Ganesh Prasad Reddy*., Professor., Department of EEE and dean of academics, Sree Vahini Institute of Science and Technology., Tiruvuru,521235, NTR District., AP. (jgpreddy@yahoo.com)
CH. Vamsi Krishna Kishore Chari, M. Mahesh Babu, G. Chandrika, K. Naveena, M. Vamsi
UG scholar students Sree Vahini institute of science and technology, Tiruvuru., NTR District., AP, India. (vamsikrishnachityala@gmail.com)

Abstract:

This research presents an innovative topology for a grid-connected wind-solar cogeneration system that is both straightforward and effective. Back-to-back voltage-source converters are used to link a full-scale wind turbine powered by a permanent magnet synchronous generator to the utility grid (VSCs). A photovoltaic solar generator has been hooked up using the DC-Link capacitor. Because no DC/DC translation stages are needed, the hybrid system is easy to use and effective. To maximize the extraction of renewable energy, the suggested topology also includes separate maximum power point tracking for the wind and solar producers. The vector control inside the rotating reference frame is used to regulate the VSCs. To describe the overall stability, the system components' comprehensive small-signal models are built. Investigated is how utility grid failures affect the effectiveness of the suggested solution. Results from nonlinear time-domain simulations conducted under various operating situations are shown to support the viability of the suggested topology

Key words: permanent magnet machines, maximum power point trackers, AC-DC power converters, DC-AC power converters, solar power generation, wind power generation

I INTRODUCTION:

During the previous ten years, the cost of wind and solar energy generation has been dramatically declining. The installed solar and wind generating capacity worldwide has exceeded 303 gigawatts (GW) and 487 GW, respectively, in 2016, driven by their technological and economic incentives, as contrasting to 6 GW and 74 GW, respectively, in 2006 [1].Power-electronic converters are used as an interfacing step to the load-side or the utility grid to construct distributed generating units due to the intermittent and uncontrolled nature of wind and solar energy [2], [3]. The majority of distributed generation systems described in the literature are entirely focused on one type of renewable resource, such as solar energy as in [4], [5], or wind energy as in [6]–[8]. Recent consideration has been given to combining solar and wind generators in one site to maximize the advantages of the available renewable resources [9]– [22].

The hybrid wind and solar energy cogeneration system has the following features: 1) The availability of wind and solar energy is often complementary, thus integrating both sources of energy boosts the total operating efficiency [23]. 2) The smaller footprint of the integrated system made possible by the hybrid wind and solar co-generators improves capital investments by maximizing the use of land resources [24]. 3) Due to the accessible moment of inertia in the mechanical components of the wind generators, the combined wind and solar cogeneration systems are more dynamically capable of supporting the utility grid than the static solar generators [8]. 4) Having two energy sources improves the reliability of the generation [9],[10]. Grid-connected wind and solar congenators are not frequently discussed in the literature [9]– [15]. For standalone off-grid applications, however, a variety of wind and solar hybrid systems are available [10], [16], and [22].

A grid-connected and stand-alone implementation of an optimum sizing technique for a wind-solar-battery system has been put out in [10]. For a hybrid system made up of the solar and wind systems, systematic stochastic planning is suggested in [11]. By using multiple-input converters, the integration of renewable energy sources has been enhanced in [12]– [14]. In [12], a fused buck/buck-boost DC-DC converter is presented. A connected transformer and a DC-DC converter with a current-source interface are presented in [13] and [14], respectively. The suggested systems are based on dc

ISSN: 2278-4632
Vol-13, Issue-03, No.02, March 2023

power distribution, which may not be the best distribution medium in ac-dominated power systems, in addition to the somewhat complicated structural topologies in [12]– [14]. Also, the systems provided are suggested for relatively low-power levels and have not been proven in high-power applications. Shown in [16, 17] is a self-contained hybrid wind and solar system that includes a diesel generator and a storage battery. On a modest scale, a single-phase hybrid system function.

Single phase hybrid system has been investigated in [18], while a laboratory-scale system is shown in [19] and [20]. A common dc-bus is frequently used in the system design in [16]–[20] to link a number of parallel converters-interfaced renewable energy resources, which may reduce overall system efficiency and increase costs [12]. The cascaded connection of power converters requires precise controller design and coordination in order to avoid the produced interactions and dynamics among the tightly controlled power converters, which might lead to instabilities [25], [26]. In order to interconnect a photovoltaic (PV) generator and an energy storage device, a back-to-back voltage-source converter (VSC) coupled to a doubly-fed induction generator is utilised in [21]. [22] proposes a wind-driven induction generator interfaced to a PV generator trying to charge a battery bank. The effective integration of renewable energy sources with the lowest use of power electronic conversion stages is highlighted by the hybrid wind-solar systems in [21], [22]. These solutions, however, are suggested for certain off-grid applications. To the best of the authors' knowledge, [15] is the primary source that addresses the grid-connected wind-solar system combo. A back-to-back VSCs is used in the system in [15] to connect the solar and wind turbines to the power grid. An outer loop proportional-and-integral (PI) dc voltage controller on the machine-side VSC regulates the dc-link voltage to the PV panel's maximum power-point tracking (MPPT) value.

A hysteresis current controller is used to regulate the machine-side currents once the reference values are determined using the synchronous detection approach. A hysteresis grid-current controller on the grid-side VSC is utilized to inject the total currents to the utility-grid. Notwithstanding the potential advantages of the approach presented in [15], the following difficulties are noted: 1) The functioning of both VSCs is required for the MPPT of either the PV or wind power, which in some circumstances may reduce the system's dependability and increase losses. For instance, the machine-side VSC may not be able to track the solar PV MPPT dc-link voltage if the wind velocity is lower than the wind turbine's cut-off speed, i.e., there is no wind power [15].2) There is no direct management of the velocity of the wind turbine, i.e., a servo operation, and the dc-link voltage is controlled from the machine side. Hysteresis controllers are used to manage the machine and grid-side currents, which results in a variable switching frequency and greater harmonic content.

This study offers a new topology, however one that is straightforward and effective to interface both the wind and solar generators into one system, motivated by the promised advantages of the hybrid wind-solar generating systems and the obstacles facing the suggested system in [15].

The following are the paper's contributions:

1) The development of grid-connected wind and solar generator combinations employing Back to Back VSCs without the need for additional power electronic switches.

2) The voltage-source rectifier (VSR) is only in charge of the wind generator's MPPT, in contrast to the suggested system in [15], whereas the voltage-source inverter (VSI) harvests the most PV power by controlling the dc-link voltage to inject the entire dc power into the utility-grid.

3) The creation of the suggested system's complete small-signal state-space model, which will be used to assess the stability of the system as a whole

4) Using time-domain simulations, the performance of the proposed hybrid system has been examined under a variety of operational situations, including utility-grid failures.

II. MODELING AND CONTROL OF THE PROPOSED HYBRID WIND-SOLAR GENERATOR

The suggested system is comprised of a VSI to link the hybrid cogeneration system to the utility grid and a VSR to interface the wind generator, as illustrated in Fig. 1. A dc line is used to connect the PV generator directly to the Back-to-Back VSCs' dc-link capacitor [27]. Each of the two two-level converters—the VSR and VSI—has six cells and an insulated-gate bipolar transistor (IGBT) connected in parallel with a diode. The full modelling and control of the suggested system are presented in the following subsections.

A. Wind generator

Due to its low operational and maintenance costs, a full-scale wind turbine (FSWT) with a permanent magnet synchronous generator (PMSG) is chosen [2]. The following is how the wind turbine model is displayed:

$$P_m = \frac{1}{2} c_p(\beta, \lambda) \rho \pi R^2 v_{wind}^3, \lambda = \frac{R_{wr}}{v_{wind}} \tag{1}$$

where Pm is the mechanical power that the wind turbine blades are able to capture, D is the air density, R is the radius of the wind turbine blade, v_{wind} is the wind speed, and Cp is the rotor power coefficient, which is a nonlinear function of the blade pitch angle and the tip-speed ratio. In order to optimise the production of wind power, is set to zero under this paper's regular working settings [13]. The following is how the PMSG is modelled:

$$\bar{v}_s = R_s i_s + L_s \frac{d\bar{\iota}_s}{dt} + jPw_r(\psi + L_s \bar{\iota}_s) \tag{2}$$

$$j \frac{d}{dt} w_r + \beta w_r = \frac{3}{2} P \varphi I_{sq} - T_m \tag{3}$$

where Vs and Is stand for the stator voltage and current in complex vector form, respectively; Rs and Ls stand for the stator-winding resistance and inductance, respectively; and x_d and x_q stand for the direct (d) and quadrature (q) components of x in the rotating reference frame. P is the number of pole pairs, Tm is the mechanical torque, j is the imaginary unit number, and F is the flux linkage of the rotor magnets. R is the mechanical speed of the rotor.

The link between the mechanical rotor speed and the power produced by the turbine at various wind speeds is seen in Fig. 2.

If the rotor speed is ideally controlled to follow the fluctuations in wind speed, the greatest amount of wind power may be produced. The MPPT for the wind generator (MPPT_W), which uses the wind speed (vw) to create the reference value of PMSG rotor speed (Wr), may be used to fulfil this job at the VSR-side, as illustrated in Fig. 1 [17], [19].

B. Machine-Side Voltage Source Rectifier (VSR)

By adjusting the mechanical rotor speed of the PMSG to match the (MPPT_W characteristics in Fig. 2, using the PI speed controller (Gs(s)) in the VSR, the greatest amount of wind power is captured (4).

$$I_{sq}^* = (w_r^* - w_r) G_s(s), I_{sd}^* = 0 \tag{4}$$

The PI speed controller is implemented in the outer loop using the formula Gs (s) = gps + gis/s, where s stands for the differential operator and the superscript "" indicates the variable's reference values. Although I_{sd} is set to zero to run at maximum generated torque, the speed controller adjusts the PMSG speed to the ideal value (r) and determines the q- component of the stator current reference (Isq).

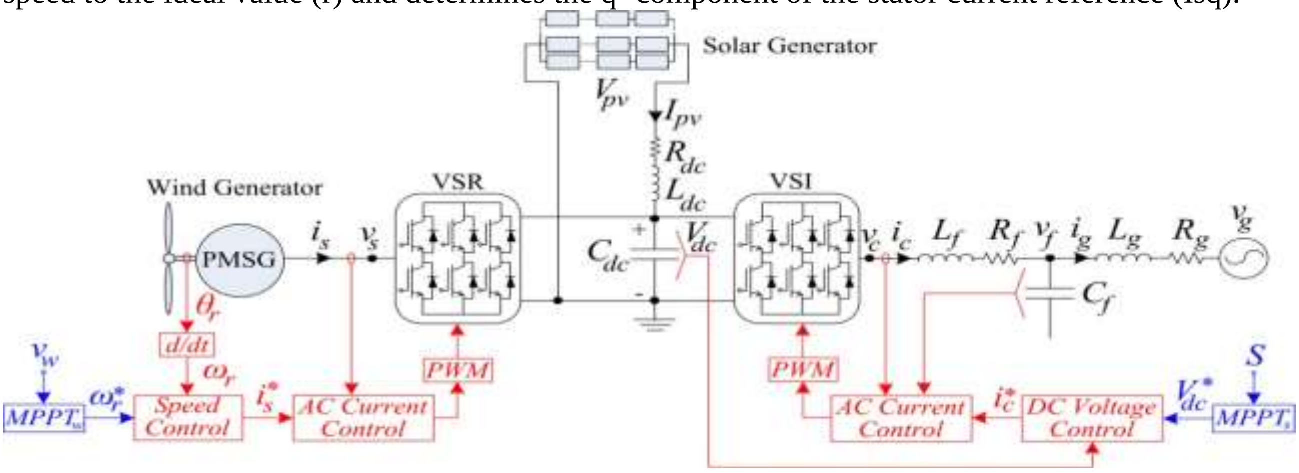

Fig. 1 Propose wind-solar cogeneration system

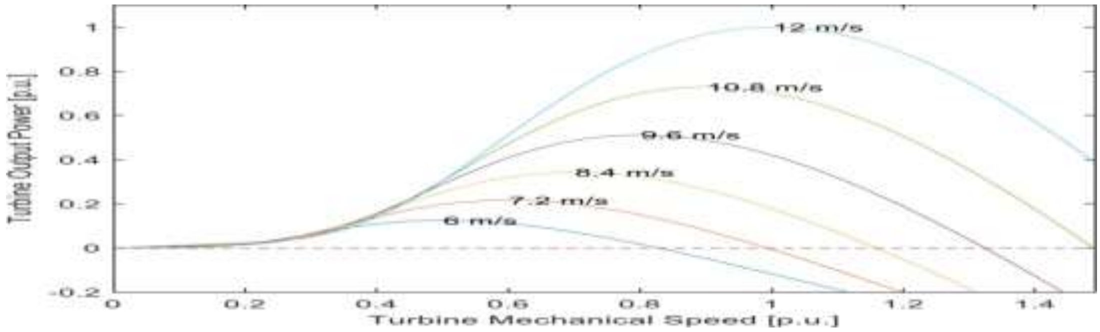

Fig.2 Mechanical characteristics of the wind turbine at different wind speeds.

Solving (3) and (4), assuming Isq ≈ I∗ sq within the bandwidth of the speed controller and setting gis/gps = β/J, the closed Loop transfer function of the speed controller (G_s (s)) becomes $\omega_r/\omega_r^* = (\frac{\frac{3}{2}P\psi g_{ps}}{J})/(s+\frac{\frac{3}{2}P\psi g_{ps}}{J}$,where the bandwidth of the speed controller is 3/2Pψgps/J [rad/s] and is selected around 0.1 of the Bandwidth of the inner PI current controller (Gi(s)) [shown in (5)]. The speed controller parameters, i.e., GPS and GIS, can be tuned accordingly

The inner loop implements the PI current controller such that the produced stator currents of the PMSG follow the relevant references in (4).

$$\bar{v}_s = (\bar{\iota}_s^* - \bar{\iota}_s)G_i(s) + jPw_r^{\circ}L_S\bar{\iota}_s + jP\psi H w_r \quad (5)$$

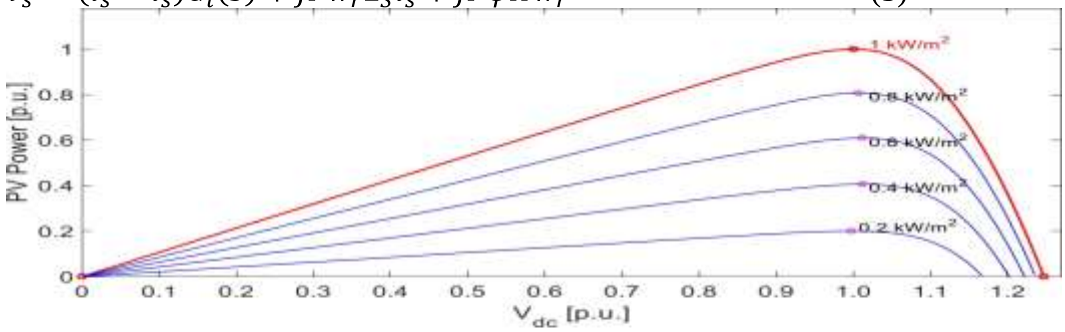

Fig. 3 Electrical characteristics of the PV array at different solar irradiance levels

Keep in mind that the decoupling loops are jPω∘ rLs, whereas the superscript "°" indicates the variable's steady-state value.

The current controller is created by resolving (2) in a manner similar to the speed controller design (5). The closed loop transfer function of the current controller is changed toI_{sd} /I_{sd}^*= 1/(Is + 1) by setting g_{ii}/g_{pi} = Rs/Ls, where the current controller's bandwidth is chosen to be between 0.1 and 0.2 of the switching frequency.

C Photovoltaic Generator

This research has taken into consideration a PV array with the model number "PV-UD190MF5" [28]. The transient stability of the system is not dynamically reflected by the PV model, despite its significant nonlinearity. The PV generator model is provided in Appendix A, and the following equations are used to represent the DC cable dynamics in Fig. 1.

$$V_{pv} = V_{dc} + R_{dc}I_{pv} + L_{dc}\, {}^{dI_{pv}}/_{dt} \quad (6)$$

Fig. 3 depicts the PV array's characteristics. There is an ideal operating point (I_{pv}, V_{pv}) where the amount of solar electricity generated is maximised at any level of solar irradiation (S). The dc-link voltage value that corresponds to the generation of the maximum PV power is chosen by the MPPT of the PV array (MPPTs) [4].

The coordination between the PV array's MPPT voltage, or Vdc, and the root-mean-square (rms) voltage at the point-of-common coupling (PCC), or $\bar{v}_f$, should be taken into account while designing the PV array. The ratio between the ac and dc voltages in the VSI in Fig. 1 determines the pulse width modulation (PWM) and switching pattern such $thatV_{c=}mv_{dc2}$, where m is the modulation signal. Any significant changes in Vdc may result in overmodulation operations or underutilized switches since Vc and Vf under steady-state conditions are largely consistent. This lowers the quality of the injected power into the utility grid. In accordance with Fig. 3, Vdc varies from 0.997 to 1.012 p.u. at various solar irradiation levels. Given the vast range of irradiance levels, it is obvious that there is only a little fluctuation in the dc-link voltage, and as a result, the effect on the switching pattern and the quality of the injected power is negligible. The nominal MPPT voltage for PV arrays is set at 1457 V, as seen in Fig. 3. PV arrays may now be directly linked to a dc-link with a nominal dc voltage of up to 1500 volts at 2.0 MVA thanks to advancements in centrally managed power converters [29].

D Grid side voltage source inverter

Figure 1 illustrates how an inductive filter (L_f) with an internal resistance (Rf) and a shunt capacitor end the ac side of the VSI (Cf). The three-phase terminal voltages and currents of the VSI have respective rms values of $\bar{v}_c$ and $\bar{\imath}_c$. Utility-grid impedance is made up of an inductive component (Lg) connected in series with the line's equivalent resistance (Rg); vg and ig are utility-grid three-phase rms.

$$\bar{v}_c = \bar{v}_f + R_f\bar{\imath}_c + L_f\frac{d\bar{\imath}_c}{dt} + \omega L_f\bar{\imath}_c \tag{7}$$

$$\bar{v}_f = \bar{v}_g + R_g\bar{\imath}_g + L_g\frac{di_g}{dt} + \omega L_g\bar{\imath}_g \tag{8}$$

$$\bar{\imath}_c = C_f\frac{dv_f}{dt} + \bar{\imath}_g + j\omega C_f\bar{v}_f \tag{9}$$

With reference to (10), the VSI is controlled by a phase-locked loop (PLL) that synchronises the converter to the utility grid [30].

$$\omega = \omega^\circ + \frac{V_{fq}^c}{V_{fq}^\circ}K_\delta(s) \tag{10}$$

The PLL structure in (10), which uses a PI controller to set the q- component of the PCC voltage (V_{cq}) to zero and produce the synchronisation angle $\delta(t)$, where $\delta(t) = \int \omega\,(t)dt$ and the superscript "c" designates the converter reference frame, implements this. While the converter is in a transient state, the angle (t) oscillates to resynchronize with the utility grid, and when the system is in a stable state, it ultimately zeros out. The decoupling between active and reactive power regulation is vector control's key benefit.

$$P_{vsi} = Real\{1.5\bar{v}_c\bar{\imath}_c^{conjugate}\} = 1.5V_{cd}I_{cd}$$

$$Q_{vsi} = Imaginary\{1.5\bar{v}_c\bar{\imath}_c^{conjugate}\} = -1.5V_{cd}I_{cd.} \tag{11}$$

In the suggested hybrid system, the VSI's functions are, in brief, 1) Production of the Maximum PV Power: This is accomplished by adjusting the Back-to-Back VSCs' (Vdc) dc-link voltage to a reference value that corresponds to the production of the maximum PV power at various solar irradiation levels. A PI controller for DC voltage$(K_{dc}(s) = K_{pdc} + \frac{K_{idc}}{s}$ therefore implemented as following;

$$I_{cd}^* = -(V_{dc}^{*2} - V_{dc}^2 K_{dc}(s)\left(\frac{1}{1.5V_{fd}^\circ}\right) \tag{12}$$

DC Power Transmission to the Utility Grid: In Fig. 1, under the assumption of a lossless converter, the balance between the supplied dc power ($P_{wind} + P_{solar}$) and the injected active power to the utility grid (P_{VSI}) determines the rate of change of the energy in C_{dc}.

$$\frac{1}{2}C_{dc}\frac{d}{dt}V_{dc}^2 = P_{wind} + P_{solar} - P_{vsi} \tag{13}$$

where$P_{wind} = Real\{1.5\bar{v}_s i_s^{conjugate}\}andP_{solar} = V_{dc}I_{pv\delta}$

In order to maintain the input-output power balance in (13) and produce the active power component (I∗ cd), the control variable in (12) is squared during regulation. The dc-link voltage controller's open-loop transfer function (K_{dc} (s)) is given by (11)– (13), were

$$l_{vdc}(s) = \frac{2K_{pdc}}{T_k C_{dc}}\left(\frac{s + \frac{K_{idc}}{K_{pdc}}}{s + \frac{1}{T_k}}\right)\frac{1}{s^2}$$

ISSN: 2278-4632
Vol-13, Issue-03, No.02, March 2023

where $\frac{1}{T_k}$ is the VSI's inner current controller's bandwidth [explained in the section below]. The $l_{vdc}(s$ contains three poles, two of which are at zero and one of which is at one $\frac{1}{-T_k}$. Because there are two poles at zero, the phase angle of $l_{vdc}(j\omega) \approx -180°$ degrees at low frequencies. As a result, the controller's settings are chosen in a way that $\frac{K_{idc}}{K_{pdc}} < \frac{1}{T_k}$.

The phase angle of lv dc (j) thus rises to its maximum value, vdc m $sin^{-1}(\frac{1-T_K\frac{K_{idc}}{K_{pdc}}}{1-T_k\frac{K_{idc}}{k_{pdc}}})$ at a specified frequency $\omega_m^{vdc} = \sqrt{\frac{2K_{pdc}}{T_k C_{dc}}}$ and asymptotically falls to close to 180. Selecting vdc-m as the cross-over frequency ensures that it will hold. $K_{pdc} = C_{dc}\omega_c^{vdc}$ like that

$$|l_{vdc}(jw_c^{vdc})| = |l_{vdc}(jw_m^{vdc})| = 1 \tag{14}$$

Hence, the phase margin is vdc m. The parameters of the DC-Link voltage controller may be found by resolving the previous equations [31]. PI ac voltage controller for PCC utility-grid voltage regulation $(K_{ac}\ (s)) = K_{pac} + \frac{K_{iac}}{s}$) The PCC voltage vf is controlled by producing Icq, which equates to the reactive power necessary to keep the PCC voltage at unity. $I_{cq}^* = -(V_{fd}^* - V_{fd}^c)K_{ac}(s)$ (15)

The PI ac current controller is used to regulate the injected currents into the utility grid $(K_i(s) = K_{pi} + \frac{K_{ii}}{s})$ as follows

$$\bar{v}_c^c = (\bar{\iota}_c^* - \bar{\iota}_c^c)K_i(s) + j\omega° L_f \bar{\iota}_c^c + \bar{v}_f^c \tag{16}$$

Kac (s) should have parameters tuned similarly to the dc voltage controller in (12), whereas Ki (s) is developed using the methodology given for Gi (s) in (5).To appropriately characterize the impact of the PLL on the system dynamics, it should be emphasized that the measured ac values (i.e., I_c and v_f) should be converted to the converter reference frame while the controller output signals (i.e., v_c) should be retransformed to the grid reference frame [30].

TABLE(1); HYBRID SYSTEM EIGENVALUES OF THE PROPOSED SYSTEM

EIGEN VALUES	INFLUENCING STTE
λ_1=-2148.6	ΔI_{sd}
λ_2=-0.52	$\Delta\gamma_{id}$
$\lambda_3 = -6.7 \times 106$	ΔI_{PV}
$\lambda_{4,5} = -56.78 \pm j42100$	ΔI_{gd},
$\lambda_{6,7} = -62.46 \pm j41400$	ΔI_{gd}, ΔI_{gg} ΔV_{fd}
λ_8=-8460	ΔI_{cd}, ΔI_{gg} ΔV_{fd}
$\lambda_9 = -4180$	ΔI_{cq}
$\lambda_{10} = -2130$	ΔI_{sq}
$\lambda_{11,12} = -139.24 \pm j59.93$	$\Delta\varphi_{vdc}$,
$\lambda_{13} = -162.31$	$\Delta\delta$
λ_{14} =**-18.**-18.93	$\Delta\omega_\gamma$
λ_{15} =**-20**-20	$\Delta\varphi_s$
λ_{16} =**-2**-2.45	

ISSN: 2278-4632
Vol-13, Issue-03, No.02, March 2023

	$\Delta\gamma_s$
λ_{17}=-0.087	$\Delta\varphi_{vac}$
λ_{18}=-0.52	$=\Delta\gamma_\omega$
$\lambda_{19}=-10$	$\Delta\varphi_\omega$, $\Delta\varphi_\omega$

With the assumption that the angle difference between the two frames is relatively small, such that cosδ -=1 and sin$\delta = 0$, the frame transformation is mathematically expressed in (16).

$$\bar{\iota}_c^c = (1 - j\delta)\bar{\iota}_c \bar{v}_f^c = (1 - j\delta)\bar{v}_f, \bar{v}_c = (1 + j\delta)\bar{v}_c^c \qquad (17)$$

III. SMALL-SIGNAL MODELING AND STABILITY ANALYSIS

The PMSG model, the VSR model and control loops, the dc-link dynamics, the VSI circuit model and controllers, the PLL controller and reference-frame transformation, and the PMSG model have all been taken into consideration while developing the small-signal model (16). The following is the final 20-state state-space model of the complete system.

$$\Delta x^{\cdot} = [A][\Delta x] \qquad (18)$$

where A, which is the state matrix, and x, which is the state vector, are both given in Appendix C. The state's (Δγid, Δγiq), Δγs , (Δϕid Δϕiq), Δϕvdc , Δϕvac , and (Δδ, Δϕδ)),denote, in turn, the integral terms of the PLL control loops, the VSR current and speed controllers, and the VSI current, dc voltage, and ac voltage controllers

A. Dominant Eigenvalues

As shown in Table I, the dynamics of the speed and current controller of the VSR, namely, Δγs ,Δγid, and Δγiq, affect the most prominent Eigenvalues and thus govern the transient performance of the suggested system. Also, the stability of the system is significantly impacted by the ac voltage controller of the VSI [state Δϕvac]]. The position of the dominant modes is associated with the controller's parameters, which are normally consistent for each mode of operation, so their migration is less likely to happen.

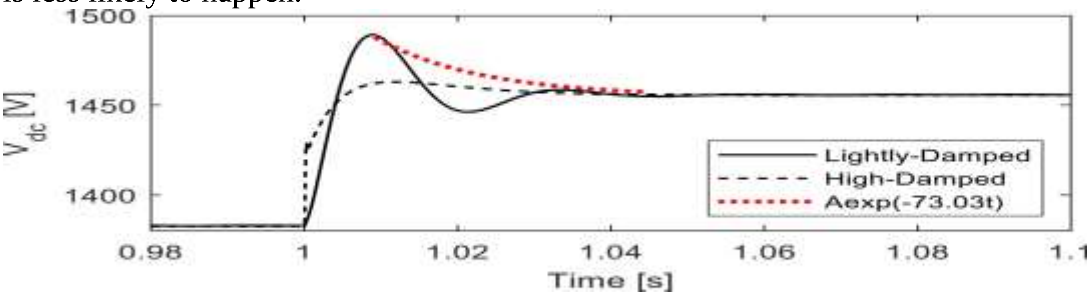

Fig.4 Step response of the dc-link voltage to verify the developed small signal model in (17).

B. *Influence of the $MPPT_W$ and MPPTs on the System Stability*

Table I demonstrates how relatively highly-damped Eigenvalues [14 and 11–12] are influenced by the states associated with the dynamics of the dc-link voltage, i.e., V 2 dc, and the mechanical speed, i.e., Δωr,. As a result, the stability of the system is not significantly affected by the driving elements for the MPPT_W and MPPTs. The fluctuation range of the ideal r and Vdc to maintain the maximum power extraction at various wind speeds and solar irradiation levels is 0.501-to1.0 p.u. and 0.997-to-1.012 p.u., respectively, according to Figs. 2 and 3. Following the ideal trace of ωr and Vdc displays little modification on the dominating modes; however, the migration of λ11, 12 and λ14 has not been greatly impacted, as predicted from the participation factor analysis in Table I.

IV. EVALUATION RESULTS

Fig. 4 validates the precision of the small-signal state-space model in (17) after a step increase in Vdc of 5.0% at t = 1.0 s. The system controllers are first built to produce a performance that is heavily damped. To make the model easier to validate, a mild damping response has been created by increasing the bandwidth of the DC-Link voltage controller. The oscillation frequency for an eigenvalue of j is [in rad/s], and the envelope of the oscillatory response decays according to the exponential function A_{exp} (t), where A is the oscillation's amplitude and t is the duration in seconds. The dominant lightly dampened mode obtained from (17) is = 73.03 j251.7. According to Fig. 4, the frequency of the oscillation of the same lightly dampened response is 247.4 rad/s, and the oscillatory response decays after closely matching A_{exp} (73.03 t). This suggests that the small-signal model in Fig. 4 was developed accurately (17).

A. ***Small-Signal Model Verification***

Fig. 4 validates the precision of the small-signal state-space model in (17) after a step increase in Vdc of 5.0% at t = 1.0 s. The system controllers are first built to produce a performance that is heavily damped. To make the model easier to validate, a gently dampened response has been created by boosting the DC-Link voltage controller's bandwidth.

The oscillation frequency for an eigenvalue of j is [in rad/s], and the envelope of the oscillatory response decays according to the exponential function A_{exp} (t), where A is the oscillation's amplitude and t is the duration in seconds.

The dominant lightly dampened mode obtained from (17) is = 73.03 j251.7 According to Fig. 4, the frequency of the oscillation of the same lightly dampened response is 247.4 rad/s, and the oscillatory response decays after closely matching A_{exp} (73.03 t). This suggests that the small-signal model in Fig. 4 was developed accurately (17).

B. ***Wind and Solar Co-Generation***

After various weather circumstances, the co-generation of solar and wind energy is examined. As seen in Fig. 6(a), for t = 2, 4, and 6 s, respectively, the wind speeds rise from 8.4 to 10.8, then fall to 7.2, and finally rise to 12 m/s. The sun's irradiance level shifts from 1 to 0.8, then 0.4, and eventually climbs to 0.6 kW/m2 at t = 3, 5, and 6 s, respectively, along with the changes in wind speed. In accordance with Figs. 2 and 3, the MPPT_W and MPPTs provide the ideal r and V dc. Figures 6 and demonstrate that both r and Vdc exhibit well-damped performance, which is evident in the produced wind and solar power (Figures 6, respectively), as well as the current that was injected into the utility grid as shown in Figure 6. For more research, the highest wind and solar power outputs of 2 MW and 0.568 MW, respectively, are created at t = 6.0 s, where the dc-link stability is maintained with a maximum overshoot of 0.06 pu. A unity PCC voltage is maintained at all times, as seen in Fig. 6. As illustrated in Figs. 6 and I, where the variable frequency functioning of the VSR is clearly indicated, the developed controllers for the hybrid wind-solar system do not saturate the pulse-width modulation of the Back-to-Back VSCs.

C. ***Wind-Only Generation***

When low irradiance conditions prevail at night, the PV generator contributes little or no electricity to the utility grid. When this occurs, the dc-link voltage controller adjusts Vdc to its lowest value in accordance with the PV characteristics shown in Fig. 3. The dc-link voltage declines to 0.858 pu. at t = 2.0 s as the PV power generation falls to zero, as illustrated in Fig. 7a), and is then restored to 1.0 pu. at t = 3.0 s as the PV power is created. Figures 7(b) and (c), respectively, depict the matching of wind and solar power as well as the injected ac current to the utility grid. Be aware that each PV string often has a blocking diode connected in series with it to stop reverse current from entering the PV array at low irradiance levels.

D. ***PV-Only Generation***

As it is expected that the wind speed will be below the cut-off speed, the bulk of the wind energy produced is lost due to system losses. As a result, the PMSG is in braking mode and uses mechanical means to stop the rotor.

ISSN: 2278-4632
Vol-13, Issue-03, No.02, March 2023

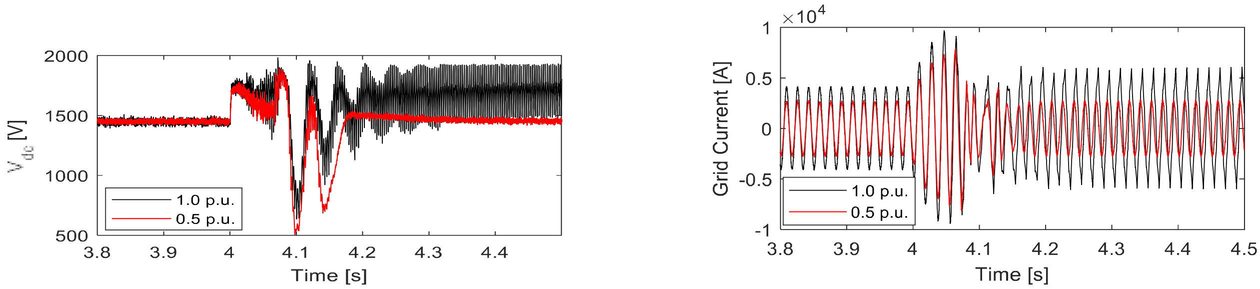

Fig. 5. Response to a 3PG fault at t = 4.0 s for 4.0 cycles – 1.0 and 0.5 pu. wind power generation with 1.0 pu. solar power.

The speed controller is used to reduce r from 1 pu. to 0, and then back to 1 pu. at t = 2 and 3 s, respectively, as illustrated in Fig. 5(a). According to Fig. 5(b), this corresponds to a sharp shift in wind speed between 0 and 1 pu. Even with the difficult operating condition, the system's stability is preserved.

E. *Co-Generation Under Utility-Grid Faults Condition*

Under short-circuit situations, converter-based distributed generation units roughly contribute at their rated currents. As a result, several utilities have mandated the fault-ride-through of power converters [32] in light of the rising integration of renewable energy supplies into electrical networks. As a result, the dispersed plants cannot be shut down during a voltage drop to zero volts that lasts for less than or equal to 150 milliseconds (9 cycles for 60 Hz systems).

In this functional scenario, the fault-ride-through capabilities of the proposed hybrid wind-solar system are examined. A 3PG fault was applied to the PCC in Fig. 1 at t = 4 s for 4.0 cycles. Moreover, pulse-width-modulated switching blocks have been used to implement the VSCs in the Simulink model. Figure 5 illustrates the utility-grid current performance at 1.0 and 0.5 pu. of wind power generation, while solar power generation is kept at 1.0 p.u.

The dc-link voltage stability is violated at 1.0 pu. wind and solar power production, and after the 3PG fault has been cleared, the quality of the injected ac current is decreased with a THD of 8.75%. The response from the 0.5 and 1.0 pu. wind and solar power production, however, shows a consistent dc-link voltage and superior current quality with a THD of 3.61%. This suggests that system instability caused by utility-grid problems may be linked to wind generators. The fault-induced abrupt reduction in PCC voltage prevents the grid from receiving the maximum amount of power from the DC-link.

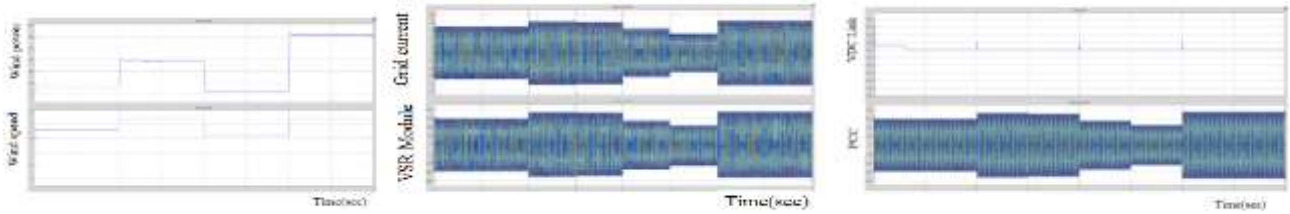

Fig. 6. Performance of the wind and solar generators

Fig. 7. Performance of the wind generator only. (a) DC-link voltage. (b) Wind and solar generated powers. (c) Injected ac current to the utility-grid.

ISSN: 2278-4632
Vol-13, Issue-03, No.02, March 2023

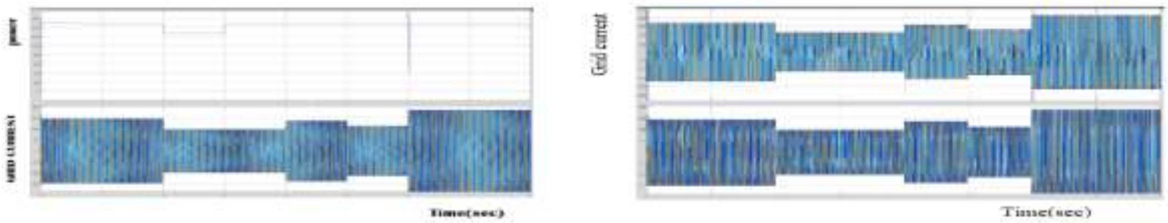

Fig. 8. Performance of the PV generator only. (a) DC-link voltage and solar generated powers. (c) Injected ac current to the utility-grid.

According to the literature, the following protection mechanisms have been activated at utility-grid fault situations to safeguard PMSG wind turbines from fault conditions [33]; 1) Dissipating the produced wind power during faults by using a brake resistance in parallel with the DC-link capacitor. 2) Using the pitch angle control to twist the wind turbine blades to limit wind power extraction and, as a result, the mechanical torque input to the PMSG. Be aware that both methods can be employed so that the mechanical pitch controller is triggered before the braking resistance produces a rapid dampening.

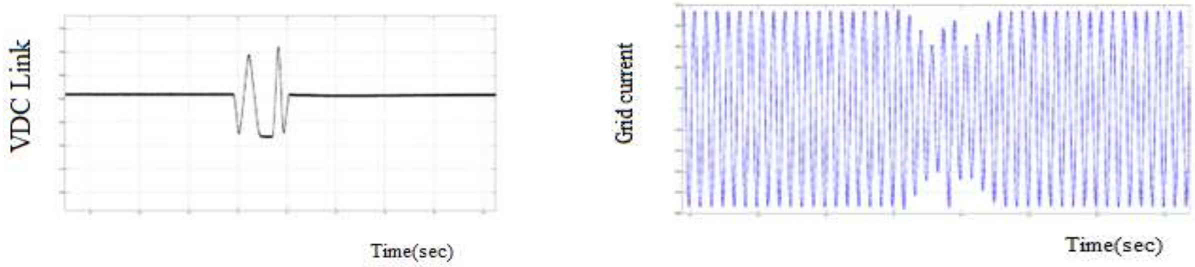

Fig. 9. Response to a 3PG fault at t = 4.0 s for 4.0 cycles – 1.0 p.u. wind and solar power generation with implemented fault protection schemes

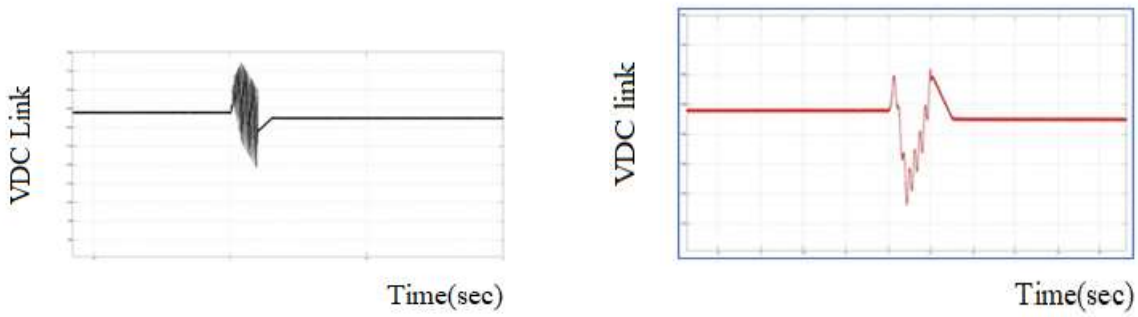

Fig. 10. Response to a 1PG fault at t = 4.0 s for 4.0 cycles – 1.0 p.u. wind and solar power generation with and without the fault protection schemes

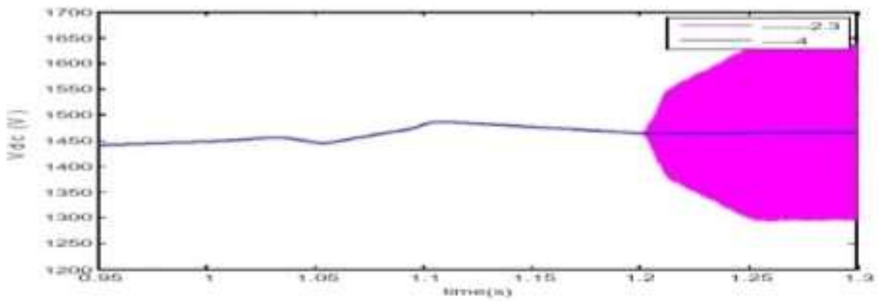

Fig. 11. DC-link voltage response at different values of SCR – 1.0 pu. solar power and a step change of the wind power from 0.5 to 1.0 pu. at t = 1 s

The input-output power balance across the dc-link capacitor is achieved by dissipating the wind power into the brake resistance and minimizing the produced wind power with the pitch angle control, enabling the fault to ride through.in Fig. 10, the system performance under single-phase-to-ground (1PG) fault circumstances is examined for further research. As compared to the 3PG faults in Fig. 5,

ISSN: 2278-4632
Vol-13, Issue-03, No.02, March 2023

it is evident that the 1PG fault has no negative effects on the system's performance. In contrast to the unprotected case, the protected system in Fig. 10 exhibits a more damped DC-Link response.

F. *Co-Generation Under Parameters Variation – Robustness*

The system's performance is steady throughout a wide range of operating points, as illustrated in Fig. 5. This section compares the system performance to changes in the parameter values. The short-circuit ratio (SCR), which measures the utility grid's stiffness, is the ratio of the utility grid's short-circuit capacity at the PCC to the rated dc power of the linked power converter. The electric grid is initially taken for granted to be robust in this research, with SCR = 15 [results in Fig. 6].

As indicated in Fig. 11, the SCR has been reduced to 4.0 and 2.3 in this part to compete with the linked converter. In both scenarios, the wind power undergoes a step increase from 0.5 to 1.0 p.u. at t = 1 s, while the solar power is kept constant at 1.0 p.u. As illustrated in Figs. 6 and 11, the system response is stable throughout a broad range of SCR values, from SCR = 15 to SCR = 4.5. Nevertheless, the interaction with the PLL dynamics causes the system to become unstable at SCR = 2.3, which is predicted at the extremely weak grid settings [7]. Fig. 12 examines the impact of CF fluctuation variations on grid voltage under the same operating circumstances.

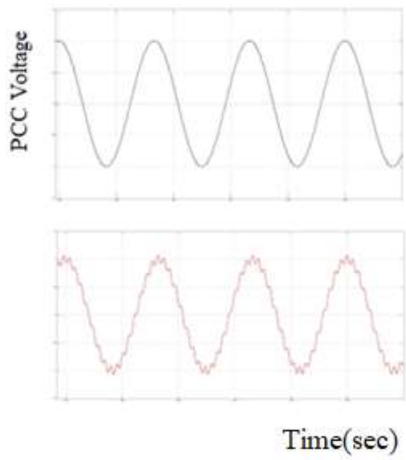

Fig. 12. PCC voltage response at different values of C_f .1.25 and 1.5

V.CONCLUSION

In this research, grid-connected Back-to-Back VSCs with vector control are used to combine wind and solar systems. After changes in wind velocity, the VSR on the wind generator side is in charge of capturing the most wind energy. On the off-grid side, the VSI's responsibilities include maximizing PV power output from the PV generator, achieving power balancing across the dc-link capacitor, and maintaining unity PCC voltage across various operating modes. To examine the system stability, a small-signal linearization study has been carried out using the whole state-space model. The suggested system has the following benefits: 1) a combination of solar and wind generators increases efficiency and dependability.2) Independent MPPT extraction, as the VSR and VSI are entirely in charge of obtaining the PV and wind energy, respectively. 3) The VSI maintains control of the DC-link voltage under all operating situations, producing improved damping performance. 4) Simple controller and system architecture 5) It is possible to implement fault-ride by utilizing the current protection protocols. The time-domain simulation results in the MATLAB/Simulink environment under various operating situations have shown a well-damped performance and an efficient operation.

APPENDIX

A. Model of the PV Generator

$$\boldsymbol{I_{pv} = N_p\left(\frac{S}{S_r}[I_{sc} + \alpha_i(t - t_r] - I_o\left[exp\left\{\frac{V_{Dq}}{n_s KAt}\right\} - 1\right] - \frac{V_D}{R_{sh}}\right)},$$

$$V_D = \frac{V_{pv} + I_{pv}\left(\frac{N_s}{N_p}\right) R_{se}}{N_s},$$

$$I_O = I_{or}\left(\frac{t}{t_r}\right) exp\left\{\frac{te_g q}{KAt}\left(\frac{1}{t_r} - \frac{1}{t}\right)\right\}$$

where I_{sc} is the PV modules short-circuit current, I is the temperature coefficient, t and tr are the actual and reference temperatures in Kelvin, and Io and Ior are the reverse saturation currents at the operational and reference temperatures, respectively. VD stands for the internal diode voltage of the PV module, q for the unit charge, K for the Boltzmann's constant, A for the ideality factor, R_{sh} and $R_{se}$for the equivalent shunt and series resistance of the PV array, e.g., for the band-gap energy of the PV cell, ns for the number of PV cells, Ns for the number of series linked modules, and Np for the number of parallel strings in the PV array.

B. System Parameter

- PMSG: Rs = 0.821 mΩ, Ls = 1.5731 mH, *P* = 26, ψ = 5.8264 Wb, *J* = 32166 kg.m2.
- VSR*:* F_{SW}= 3420 Hz, Gs(*s*) = 3000 + 6500/s, *Gi*(*s*) = 3.38 + 1.76/s, and *H* = 1.
- PV: *Np* = 83, *Ns* = 59, ns = 50, R_{dc}= 0.125 mΩ,L_{dc}= 0.34 μH.
- DC-Link: C_{dc}= 4.7 mF.
- $VSIF_{sw}$=3420 Hz, Rf = 3 mΩ, Lf = 0.3 mH, Cf = 60μF, Kδ(*s*) = 180 + 3200/s, K_{dc} (*s*) = 1 + 100/s,

Kac (s) = 0.001 + 24/s, and Ki(s) = 1.289 + 12.89/s.
- Utility-Grid*:* V_f= 600 V, MVA_{sc}= 100 MVA, X/R

Ratio = 10.3420 Hz, Rf = 3 mΩ, Lf= 0.3 mH C

BIBLIOGRAPHY:

- *[1*] Renewable Energy Policy Network for the 21st Century, "*Advancing the global renewable energy transition," REN21 Secretariat, Paris, France, 2017.* [Online]. Available: http://www.ren21.net/wpcontent/uploads/2017/06/GSR2017 -Highlights.pdf
- [2] F. Blaabjerg, Z. Chen, and S. B. Kjaer, "*Power electronics as efficient interface in dispersed power generation systems,*" IEEE Trans. Power Electron., vol. 19, no. 5, pp. 1184–1194, Sep. 2004.
- [3] J. Carrasco et al., "*Power-electronic systems for the grid integration of renewable energy sources—a survey*," IEEE Trans. Ind. Electron., vol. 53, no. 4, pp. 1002–1016, Jan. 2006.
- [4] A. Yazdani and P. P. Dash, "*A control methodology and characterization of dynamics for a photovoltaic (PV) system interfaced with a network*," IEEE Trans. Power Del., vol. 24, no. 3, pp. 1538–1551, Jul. 2009 distribution
- [5] L. Nousiainen et al., "*Photovoltaic generator as an input source for power electronic converters*," IEEE Trans. Power Electron., vol. 28, no. 6, pp. 3028–3038, Jun. 2013.
- [6] N. Strachan and D. Jovicic, "*Stability of a variable-speed permanent magnet wind generator with weak ac grids,*" IEEE Trans. Power Del., vol. 25, no. 4, pp. 2279–2788, Oct. 2010.
- [7] P. Mitra, L. Zhang, and L. Harnefors, "*Offshore wind integration to a weak grid by VSC-HVDC links using power-synchronization control— A case study*," IEEE Trans. Power Del., vol. 29, no. 1, pp. 453–461, Feb. 2014.
- [8] Y. Wang, J. Meng, X. Zhang, and L. Xu, "*Control of PMSGbased wind turbines for system inertial response and power oscillation damping,*" IEEE Trans. Sustain. Energy, vol. 6, no. 2, pp. 565–574, Apr. 2015.
- [9] F. Giraud, "*Analysis of a utility-interactive wind-photovoltaic hybrid system with battery storage using neural network,*" Ph.D. dissertation, Dept. Electr. Eng., Univ. Massachusetts Lowell, Lowell, MA, USA, 1999.
- [10] L. Xu, X. Ruane, C. Mao, B. Zhang, and Y. Luo, "*An improved optimal sizing method for wind-solar-battery hybrid power system*," IEEE Trans. Sustain. Energy, vol. 4, no. 3, pp. 774–785, Jul. 2013.

- [11] S. Sarkar and V. Ajjarapu, "*MW resource assessment model for a hybrid energy conversion system with wind and solar resources,*" IEEE Trans. Sustain. Energy, vol. 2, no. 4, pp. 383–391, Oct. 2011.
- [12] Y.-M. Chen, Y.-C. Liu, S.-C. Hung, and C.-S. Cheng, "*Multi-input inverter for grid-connected hybrid PV/wind power system*," IEEE Trans. Power Electron., vol. 22, no. 3, pp. 1070–1077, May 2007.
- [13] S. Bae and A. Kwasinski, "*Dynamic modelling and operation strategy for microgrid with wind and photovoltaic resources,*" IEEE Trans. Smart Grid, vol. 3, no. 4, pp. 1867–1876, Dec. 2012.
- [14] B. Mangu, S. Akshatha, D. Suryanarayana, and B. G. Fernandes, "*Grid-connected PV-wind-battery-based multi-input transformer-coupled bidirectional dc-dc converter for household applications*," IEEE Trans. Emerg. Sel. Topics Power Electron., vol. 4, no. 3, pp. 1086–1095, Sep. 2016.
- [15] P. Shanthi, G. Uma, and M. S. Keerthana, "*Effective power transfer scheme for a grid connected hybrid wind/photovoltaic system,*" IET Renew. Power Gener., vol. 11, no. 7, pp. 1005–1017, 2017.
- [16] T. Hirose and H. Matsuo, "*Standalone hybrid wind-solar power generation system applying dump power control without dump load,*" IEEE Trans. Ind. Electron., vol. 59, no. 2, pp. 988–997, Feb. 2012.
- [17] K. Kant, C. Jain, and B. Singh, "*A hybrid diesel-wind-PV based energy generation system with brushless generators*," IEEE Trans. Ind. Inf., vol. 13, no. 4, pp. 1714–1722, Aug. 2017. [18] U. Kalla, B. Singh, S. Murthy, C. Jain, and K. Kant, "*Adaptive sliding mode control of standalone single-phase microgrid using hydro, wind and solar PV array-based generation*," IEEE Trans. Smart Grid., vol. 9, no. 6, pp. 6806–6814, Nov. 2018.
- [19] A. Merabet, K. Ahmed, H. Ibrahim, R. Beguenane, and A. Ghia's, "*Energy management and control system for laboratory scale microgrid based wind-PV-battery*," IEEE Trans. Sustain. Energy, vol. 8, no. 1, pp. 145– 154, Jan. 2017.
- [20] M. Meiqin, S. Jianhui, L. Chang, Z. Guorong, and Z. Yuzhu, "*Controller for 1 kW–5 kW wind-solar hybrid generation systems*," in Proc. Can. Conf. Elect. Comput. Eng., Niagara Falls, ON, Canada, 2008, pp. 1175–1178.
- [21] A. Hamadi, S. Rahman, K. Eddowes, and K. Al-Haddad, "*A modelling and control of DFIG wind and PV solar energy source generation feeding four wire isolated load*," in Proc. Annu. Conf. IEEE Ind. Electron. Soc., Vienna, Austria, 2013, pp. 7778–7783.
- [22] S. Daniel and N. Ammasai Gounden, "*A novel hybrid isolated generating system based on PV fed inverter-assisted wind-driven induction generator*," IEEE Trans. Energy Convers., vol. 19, no. 2, pp. 416–422, Jun. 2004.
- [23] P. E. Bett and H. E. Thornton, "*The climatological relationships between wind and solar energy in Britain*," Renewable Energy, vol. 87, no. 1, pp. 96–110, 2016.
- [24] S. Shanghvi, W. M. Grady, and B. Schwarz, "*Evaluating the impact of wind turbine shadows on an integrated wind and solar farm,*" in Proc. 3rd IEEE PES Innovative Smart Grid Technol. Eur., Berlin, Germany, 2012, pp. 1–6.
- [25] J. Zhang, X. Xie, D. Jiao, and Z. Qian, "*Stability problems and input impedance improvement for cascaded power electronic systems*," in Proc. 9th Annu. IEEE Appl. Power Electron. Conf. Expo., 2004, vol. 2, pp. 1018– 1024.
- [26] A. Radwan, "*Modelling, analysis and stabilization of converter-dominated power distribution grids,*" M.Sc. thesis, Dept. Electr. Comput. Eng., Univ. Alberta, Edmonton, AB, Canada, 2012.
- [27] D. Salomon son, L. Sodder, and A. Santino, "*Projection of low-voltage ¨ dc microgrid*," IEEE Trans. Power Del., vol. 24, no. 3, pp. 1045–1053, Jul. 2009.
- [28] PV-UD190MF5, *Mitsubishi, San Francisco*, CA, USA, 2007.
- [29] ABB Solar Inverters, "*PVS980*," ABB, Zurich, Switzerland, 2018. ¨
- [30] L. Hereford, M. Buongiorno, and S. Lundberg, "*Input-admittance calculation and shaping for controlled voltage-source converters,*" IEEE Trans. Ind. Electron., vol. 54, no. 6, pp. 3323–3334, Dec. 2007.
- [31] A. Yazdani and R. Iravani, Voltage-Sourced Converters in Power Systems—Modelling, Control, and Applications. Hoboken, NJ, USA: Wiley, 2010.
- [32] E. Troester, "*New German grid codes for connecting PV systems to the medium voltage power grid*," in Proc. 2nd Int. Workshop Concentrating Photovoltaic. Power Plant, pp. 1–4, 2008.
  - [33] I. Abdelsalam, G. Adam, and B. Williams, "*Current source back-to-back converter for wind energy conversion systems*," IET Renew. Power Gener., vol. 10, no. 10, pp. 1552–1561, 2016.